# Structure and dynamics of breaking foams

G. D. Burnett, J. J. Chae, and W. Y. Tam*
*Department of Physics, University of Arizona, Tucson, Arizona 85721*

Rita M. C. de Almeida
*Instituto de Fisica, Universidade Federal do Rio Grande do Sol, Caixa Postal 15051, 91501-970 Porto Alegre, Brazil*

M. Tabor
*Program in Applied Mathematics, University of Arizona, Tucson, Arizona 85721*
(Received 1 November 1994)

Experimental results are presented for the relaxation of a two dimensional soap foam in which wall breakage is initiated through gentle warming of the foam cell. Significantly different phenomenology from the relaxation of nonbreaking foams is observed. At a critical "break time," which depends on the temperature ramping rate and initial conditions, a large scale mechanical cascade of wall rupture sets in, leading to a rapid disintegration of the foam. In the cascade regime, whose behavior is essentially independent of the ramping rate, a dynamical scaling behavior, associated with the distribution of cell edge lengths, is proposed.

PACS number(s): 82.70.Rr, 83.70.Hq

## I. INTRODUCTION

Although the structure of evolving soap foams in two dimensions has been recognized for quite some time to provide valuable models of cellular structures ranging from biological tissue to metallic grain boundaries [1], it is only more recently that a reasonable number of detailed experimental [2–4], theoretical [5–9], and numerical [10–15] studies have been performed. (A recent review has been provided by Glazier and Weaire [16].) The basic dynamics is driven by the pressure difference across the cell boundaries and recognition of this led von Neumann to his famous law for the evolution of bubble area, namely an $n$-sided bubble of area $a_n$ evolves as

$$\frac{da_n}{dt}=\kappa(n-6)\ , \tag{1}$$

where $\kappa$ is a diffusion coefficient. Thus bubbles of five or less sides shrink and those of seven or more sides grow—a result that is borne out, for the most part, experimentally. An important ingredient of the model is that the angle between the walls joining at a vertex is 120°. When such a foam becomes relatively "wet," Plateau borders form around the vertices and change the angles from 120°. The way in which this influences the cell evolution has been studied by Bolton and Weaire [12]. The actual foam evolution is governed by more than just the von Neumann equation (1) and must be coupled with two topological processes. These are the $T2$ transition(s) which correspond to the rearrangement of cell walls when the bubble to which they are attached shrinks to zero and the $T1$ process which corresponds to a wall "switching." Both processes are important in correctly describing foam evolution and the $T1$ transitions, in particular, may have quite long range effects as has been demonstrated, for example, in the numerical simulations of Herdtle and Aref [10]. One of the most important dynamical scaling laws is the prediction [16] (based on a simple dimensional analysis) that the mean cell area $\langle a \rangle$ grows as $t^{1.0}$ leading to the so called "scaling regime" in which all distributions, such as the normalized area distribution $P(a/\langle a \rangle, t)$, are stationary.

Here we describe results on the dynamics of *breaking foams,* namely foams in which wall rupture—hitherto avoided—is included as one of the critical dynamical processes. The dynamics of such foams will be shown to be significantly different from the more traditional class and raises a host of fascinating questions. There are a variety of motivations for studying breaking foams. These range from models of evolving biological structures [17,18] to the breakup of environmentally offensive effluent scum.

## II. EXPERIMENTAL OBSERVATIONS OF BREAKING FOAMS

In our experiments, cell breaking is caused by the effect of gentle heating which is, in fact, provided by nothing more than the heat generated by the light box used to illuminate the cell containing the foam. Two thick, circular, Plexiglas plates form the walls of the cell and washers sandwiched between the plates set the spacing between the plates. The cell is sealed with an O-ring forming a circular cavity of diameter 26.35 cm ($10\frac{3}{8}$ in.) and gap 0.238 cm ($\frac{3}{32}$ in.) The cavity volume is 129.82 cm$^3$. A thermistor is attached to the bottom plate to monitor the temperature of the cell. High purity sodium dodecyl sul-

*Present address: Department of Physics, The Hong Kong University of Science and Technology, Clear Water Bay, Kowloon, Hong Kong.

 

fate in distilled water at a concentration of $0.02M$ is used as the soap solution. In order to prepare a foam a small volume of this solution is introduced into the cell. The foam can then be generated by use of a peristaltic pump (for a uniform initial bubble pattern) or by vigorous manual shaking of the chamber (for more random initial conditions). If the latter method is used, small nuts, which are placed in the chamber, act as agitators and have the effect of randomly drawing out single films which help produce the full foam network. When a reasonable foam configuration has been achieved, some of the fluid in the cell may be drawn off to create a desired degree of foam "wetness" which can be approximately controlled by measurement of the amount of fluid initially introduced and finally removed. A coarse measure of this is provided by the total liquid to cavity ratio and a finer scale measure is provided by the typical size of the Plateau borders. The thickness of the cell walls makes accurate measurement of the borders by conventional optics quite difficult but rough estimates can be made and are certainly clear to the eye. In what follows we will describe experiments performed with a relatively "dry" foam, which corresponds to a liquid content of 0.3–0.4 $cm^3$ and a typical initial Plateau border size of 150 $\mu$m, and a relatively "wet" foam with a liquid content of 3.0 $cm^3$ and border size of 350 $\mu$m. It may be assumed that, unless otherwise stated, all runs described correspond to the dry foam.

Complete control over the initial foam configuration, in terms of bubble area and distribution statistics, is essentially impossible but with practice approximately similar looking distributions in terms of bubble area, number, and randomness can be generated as well as those with more or less bubbles.

After allowing the newly generated foam to relax for a while (to establish a uniform drainage of fluid throughout the foam) the chamber is mounted horizontally above a light box. Plates of various color and composition are placed between the light box and chamber. This, combined with different choices of bulbs in the light box itself, enables one to produce a variety of different temperature ramping rates. This rather unsophisticated arrangement is both surprisingly reproducible and, for our current purposes, perfectly adequate since, as we will describe, the actual breakdown cascade—which is our primary interest here—appears to be reasonably independent of the ramping rate. The three different rates used in our experiments are shown in Fig. 1. For convenience we will refer to the three rates, in obvious order, as "low," "medium," and "high." Further studies with more finely controlled ramping mechanisms will be described elsewhere [19]. The foam chamber is illuminated from above with a circular fluorescent bulb which gives excellent contrast of the foam network in two dimensions. A charge coupled device (CCD) camera with (640×480) pixel resolution mounted above the assembly is then used to either grab individual frames for direct storage in digitized form on a computer or feed directly to a VCR, from which individual frames can be subsequently taken for analysis. A variety of programs were developed to analyze the digitized images, e.g., to find the

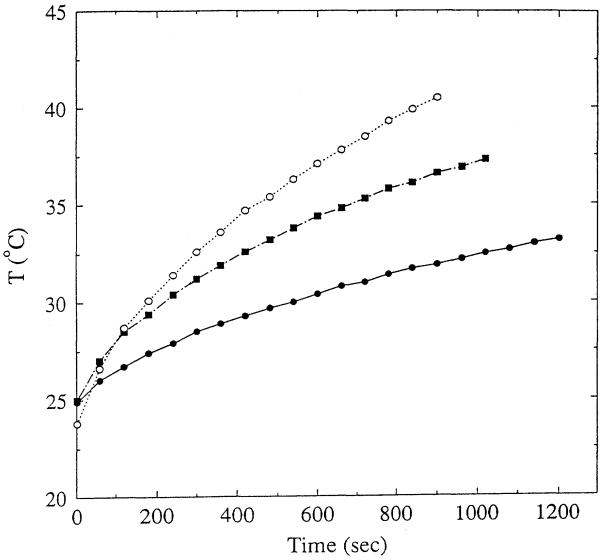


FIG. 1. Temperature ramping rates used in experiment; ●, low ramping rate; ■, medium ramping rate; ○, high ramping rate.

area of individual cells and the number of length of their sides.

A typical evolution sequence is shown in Fig. 2 corresponding to a (dry) foam with an initial bubble count of approximately 2000 bubbles and the medium ramping rate shown in Fig. 1. It must be emphasized that whereas a normal foam relaxation without wall rupture proceeds over time scales of tens of hours, the breaking foam dynamics is completed in tens of minutes. During the first few minutes the cellular patterns [Figs. 2(a) and Fig. 2(b)] appear little different from those that might be seen in traditional nonbreaking foams. There are a few rearrangements due to the breakage of tiny three dimensional bubbles, nestled in the Plateau borders, which triggers off some $T1$ transitions in the immediate neighborhood. By Fig. 2(c), however, wall rapture takes over as a major mechanism and the subsequent sequence of cell patterns is radically different from regular evolution. The breakdown is characterized by a cascade of wall rupture with the breakage of cell walls causing large scale rearrangements of neighboring cells which in turn generate long range stresses over the network resulting in further breakage and hence rapid breakdown. The cascade and its long range correlations become particularly clear when the recorded runs are played back at high speed. The latter stages of the foam are characterized by narrow, isthmuslike regions of small bubbles into which much of the liquid from the broken walls has drained. As will be described in some detail below, the "breakdown cascade" appears to have two key features: (i) a critical "break time" which marks its onset and is sensitive to ramping rate and initial conditions, and (ii) a subsequent "universal" behavior, for a period of time, that appears to be independent of initial conditions.

Observation of individual cell wall breakage is difficult since these occur at (very) high speed. A casual distinc-

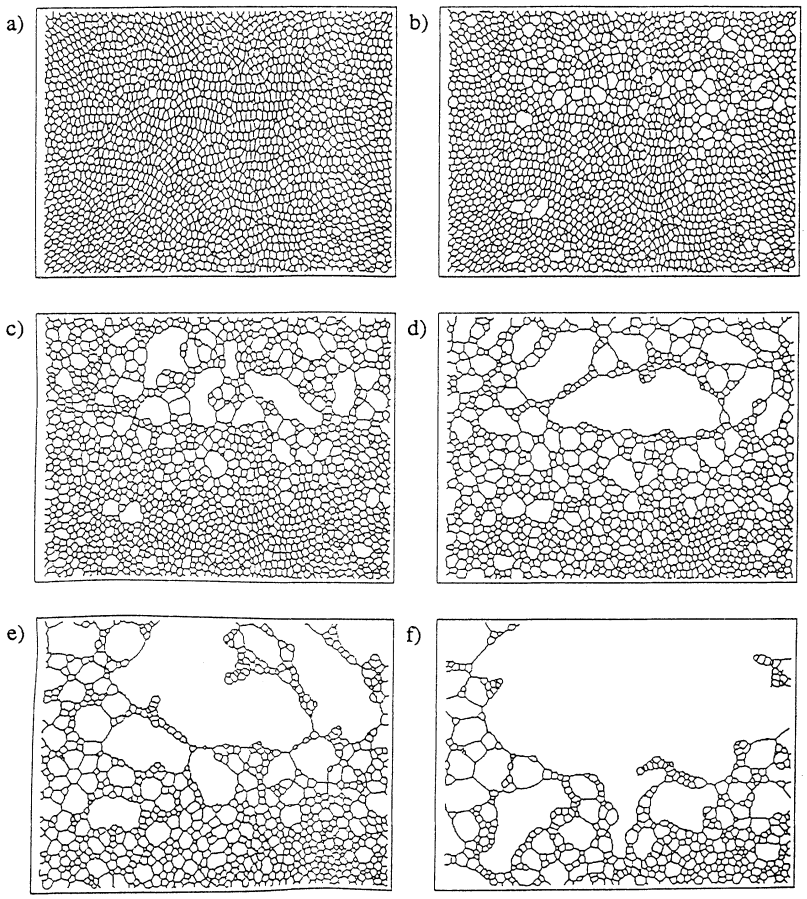


FIG. 2. Sequence of enhanced images of a breaking foam at $t =$(a) 290 sec, (b) 590 sec, (c) 690 sec, (d) 750 sec, (e) 790 sec, and (f) 850 sec.

tion can be made between those breakages corresponding to the "snapping" of long, relatively straight, cell walls between bubbles of similar area and the "popping" of rather small bubbles at the periphery of larger bubbles.

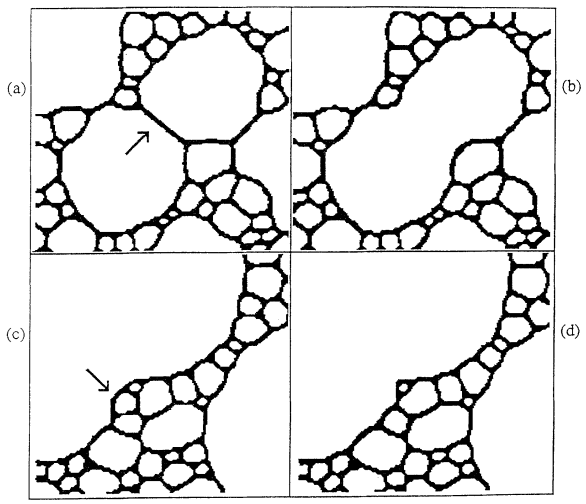


FIG. 3. Breaking a single film, where (a) and (b) show sequential images of the snapping of a long film and (c) and (d) show the bursting of a small bubble. Arrows indicate the breaking film.

These two sequences are captured in Fig. 3. However, as will be discussed later, we have little understanding of the precise mechanisms governing the cell wall rapture and hence, at this stage, do not claim any real distinction between these behaviors. A rather entertaining phenomenon observed in our experiments with wet foams is the appearance and movement of two-sided bubbles. The reason why we claim the appearance of such bubbles is as follows. Not infrequently a cell wall connected to a (usually small) three-sided bubble breaks, leaving behind

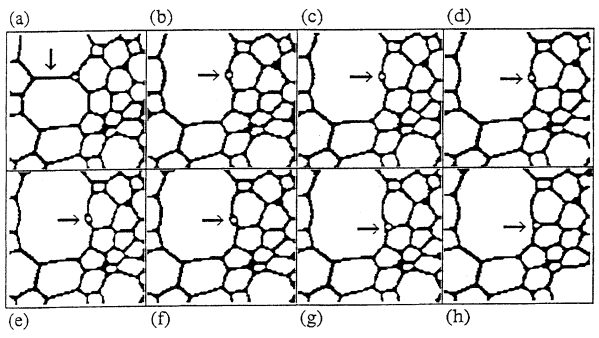


FIG. 4. Creation and motion of a two-sided bubble in a wet foam. The arrows indicate the breaking of the initial three-sided bubble and the subsequent motion of the two-sided bubble.

a small elliptical shaped cell with walls emanating from both ends—it is this entity that we call a two-sided bubble. Such a bubble then "slides" down one of these two walls towards a vertex. On reaching the vertex it then appears to "fill" that region, giving the appearance of a three-sided bubble which then rapidly shrinks to zero. This sequence is shown in Fig. 4. It is also possible for two-sided bubbles to appear in the dry foam experiments. However, because of the dryness of the film on which the two-sided bubbles reside, there is no fluid mechanism allowing movement of the bubble towards a vertex. The bubble remains stationary until one of its supporting film walls breaks. The remaining supporting wall then collapses back into the isthmus of bubbles it projects from, carrying with it the bubble which is then "absorbed" by the isthmus.

The experiments were repeated for the three different ramping rates shown in Fig. 1, for different initial conditions characterized by initial bubble number and different degrees of foam wetness. The gross, configurational phenomenology, as characterized by the Fig. 2 sequence, is always about the same; it is the more detailed dynamics, such as the onset of the breakdown cascade and certain other statistics, that are initial condition dependent. Results were found to have some sensitivity to the age (in terms of weeks) of the soap solution and the final sets of runs presented here were all performed with solutions of approximately (in terms of days) the same age.

## III. ANALYSIS OF EXPERIMENTAL RESULTS

One of the most obvious consequences of wall rupture is the overall and rapid reduction in the total number of bubbles. In Fig. 5 we show the bubble count as a function of time for the three different ramping rates. Immediately apparent is the idea of the critical break time which marks the beginning of a rapid depreciation of total bubble count: the higher the ramping rate, the earlier the process begins. This break time is also sensitive to initial conditions at a given ramping rate. In Fig. 6 we show, for runs at the medium ramping rate, the total bubble count for three different initial conditions corresponding to different initial bubble number: the smaller the initial bubble density, the shorter the break time. The effect of foam wetness on the process is shown in Fig. 7. The evolution of the wet and dry foams with the same ramping rate and approximately the same initial bubble density shows that the break time is significantly earlier for the

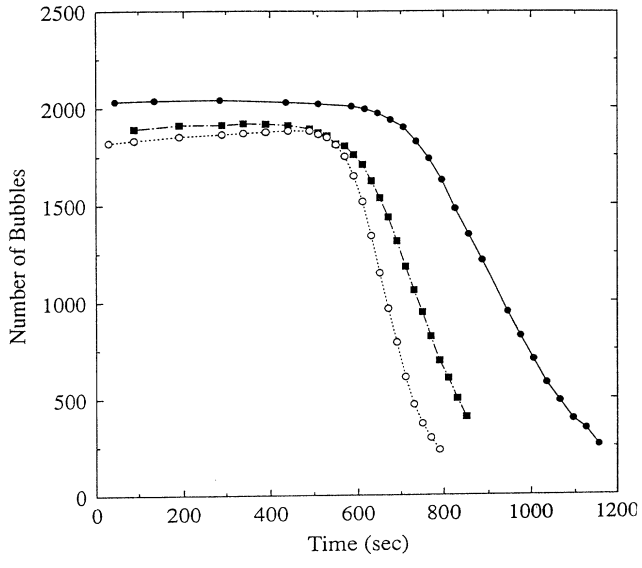


FIG. 5. Number of bubbles ($N$) as a function of time for the three distinct ramping rates for a dry foam; ●, low ramping rate; ■, medium ramping rate; ○, high ramping rate.

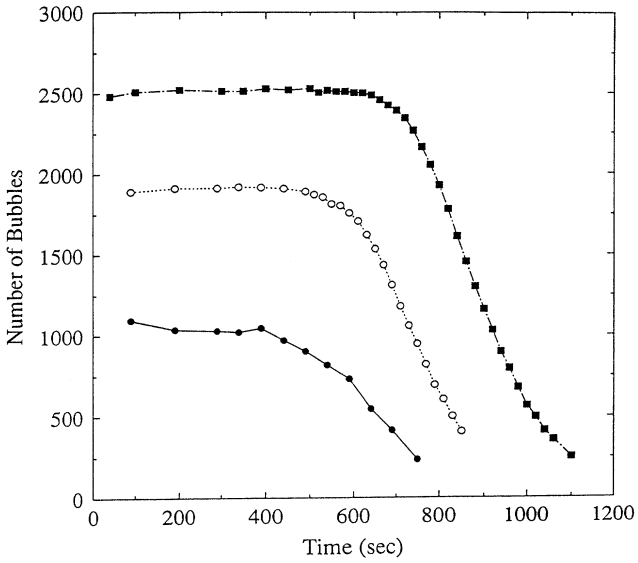


FIG. 6. Number of bubbles ($N$) as a function of time for a dry foam for varying initial bubble density. The ramping conditions (medium) are the same in each run.

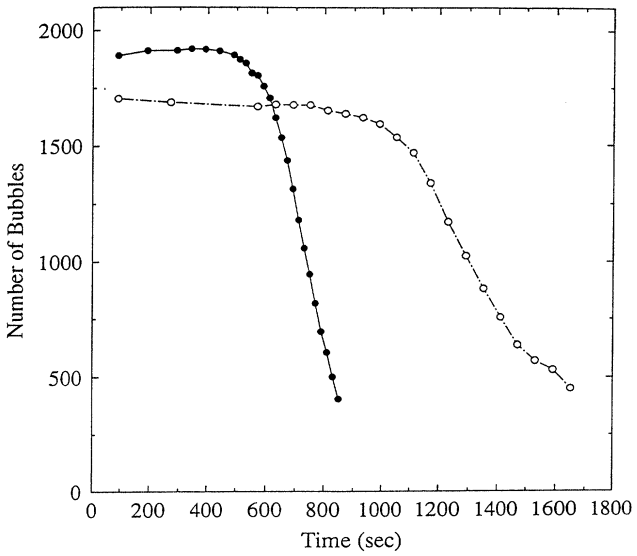


FIG. 7. Number of bubbles ($N$) as function of time for both a wet and a dry foam at same (medium) ramping rate.

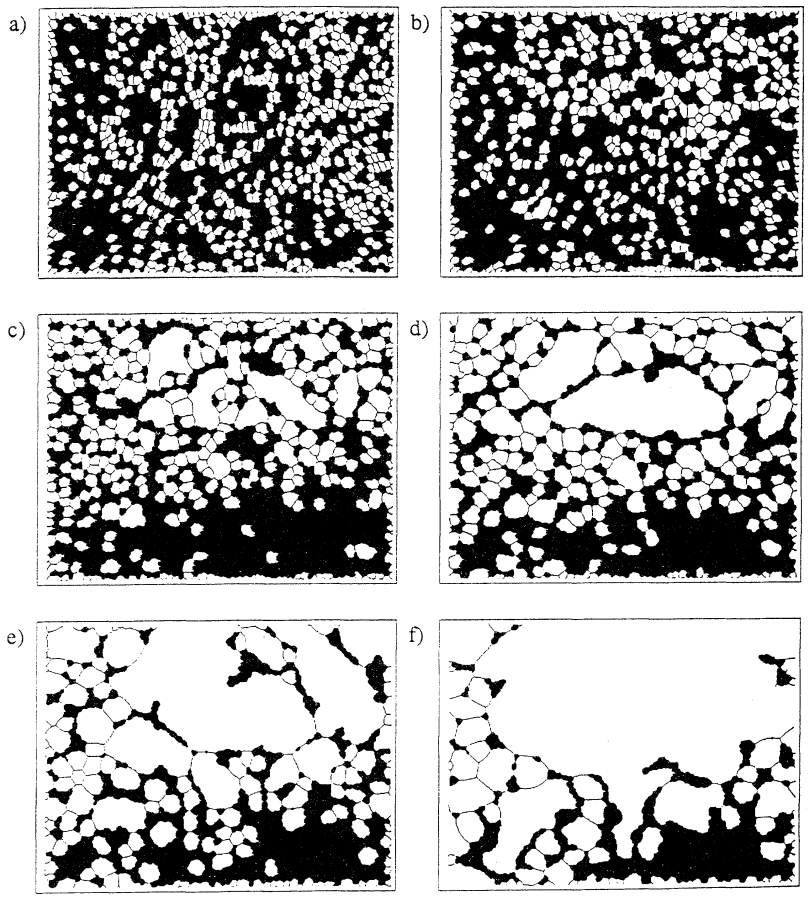


FIG. 8. Sequence of covered area images of a breaking foam at $t = 290$ sec (a), 590 sec (b), 690 sec (c), 750 sec (d), 790 sec (e), and 850 sec (f). Black regions correspond to bubbles of size less than or equal to the mean bubble area.

drier foam.

A statistic that is helpful in capturing, if not defining, the essence of the process, i.e., a breakdown cascade initiated at a critical time, is that of "percentage area covered" (PAC). Unlike regular foams one can clearly see during the evolution the emergence of regions of the experimental cell that are either covered, or not covered, by foam. This is brought out clearly by defining the PAC as the area covered by bubbles of area less than the mean. (This choice helps eliminate the ambiguity between identifying a region that is definitely devoid of foam as opposed to that which just corresponds to the space inside a whole bubble.) In Fig. 8 we show the experimental sequence of Fig. 2 in which the bubbles of less than mean area are now shaded black. In the end the picture is dominated by the black regions corresponding to the isthmuslike regions of small bubbles described earlier. Most striking, however, is the plot, shown in Fig. 9, of PAC as a function of time for the three different ramping rates. This again reinforces the idea of a critical break time after which the cascade of wall rupture takes over the decimates the foam. As one might expect, the break time is shorter for higher ramping rates. However, once past the break time, the foam disintegration—as captured by the PAC statistic—shows, for the different

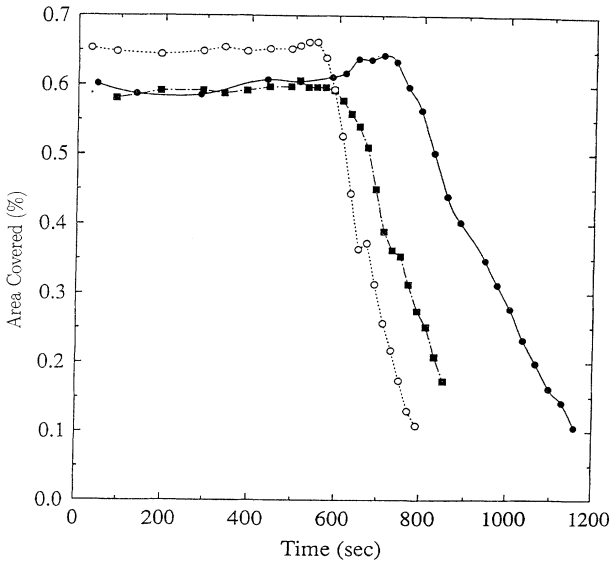


FIG. 9. Covered area as a function of time for the three distinct ramping rates shown in Fig. 1; ●, low ramping rate; ■, medium ramping rate; ○, high ramping rate.

ramping rates, similar behavior. This is manifested, at first, by approximately similar (steep) slopes followed by a distinct slowing down of PAC decrease.

All this suggests, as will be discussed in more detail below, that the process can be broken into three reasonably distinct phases.

(i) The initial warming of the foam which results, as a consequence of complex physical chemistry, in a sufficient weakening of the cell walls to make them susceptible to rupture.

(ii) The subsequent breakdown cascade which appears to be dominated by the mechanics of stress transmission through a complex network. We identify the cascade regime with the period, after the break time, for which the disintegrating network still remains effectively "connected". We will argue that this phase of the evolution exhibits a certain scaling behavior.

(iii) A final period, manifested by the slowing down of the decrease in PAC. This seems to be associated with the phase in which the foam has broken up into distinct regions, all of which are relatively wet due to collection of fluid in the walls and vertices of the bubbles. The disconnectedness of the foam reduces the range of stress transmission and the increase of wetness decreases the mobility of the cell walls.

One of the standard ways of characterizing the evolution of a nonbreaking foam is through the behavior of the cell area and its distribution function. As is easily imagined, rupture allows for the rapid creation of cells with large numbers of sides and large area, although many very small cells are still present. In Fig. 10 we show plots of mean cell area $\langle a \rangle$ versus time. They show, after an initial period of very slow growth, the expected break time heralding a period of rapid growth corresponding to the breakdown cascade. The behavior shown is reminiscent of that displayed by magnetic bubbles subjected to increasing external magnetic field [13] and quite different from the linear growth found in the scaling regime of nonbreaking foams. In Fig. 11 we show, for the medium ramping rate, a sequence of probability distributions of (normalized) area, namely $P(a/\langle a \rangle, t)$ at different times. Inevitably the breaking foams show a long tail corresponding large $a/\langle a \rangle$. The distributions also show, at later times, a shift towards smaller bubble areas reflecting the structure of the regions remaining after the main disintegration cascade. Perhaps most significant is the steady shift in time implying no stationarity of distribution—even over the narrow time band, whose significance will become clear shortly, shown in Fig. 11(b). We also mention that all the distributions indicate a characteristic length scale at each instant of time and hence, as with regular foams, that breaking foam structures are not spatially self-similar.

In Fig. 12 we show a matching sequence of probability distributions, $P(n,t)$, of the numbers of cell sides. Although exhibiting an initially strong peak around $n=6$ they exhibit the expected long tail corresponding to the formation of large cells with very large numbers of sides. Nonetheless, as time evolves there is a definite shift in favor of bubbles of small side number which corresponds to the fact that the (few) very large bubbles are surrounded by many few-sided (and small area) bubbles.

The distribution functions $P(a/\langle a \rangle, t)$ and $P(n,t)$ capture the inevitable consequences of wall rupture, namely, the appearance of bubbles with large area and

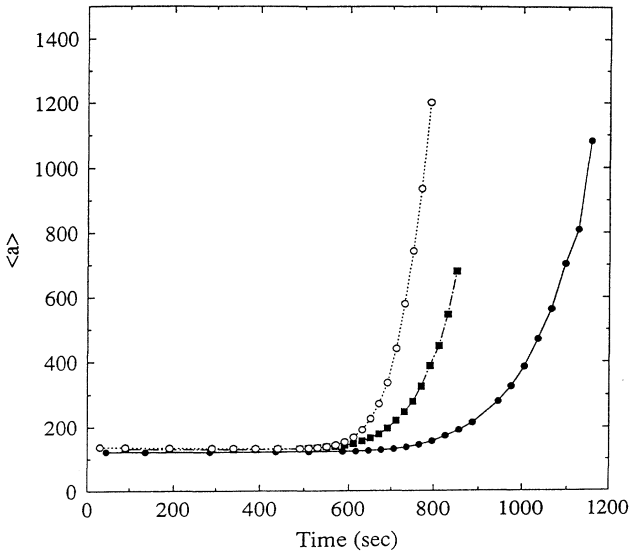


FIG. 10. Mean area as a function of time for the three distinct ramping rates shown in Fig. 1; ●, low ramping rate; ■ medium ramping rate; ○, high ramping rate.

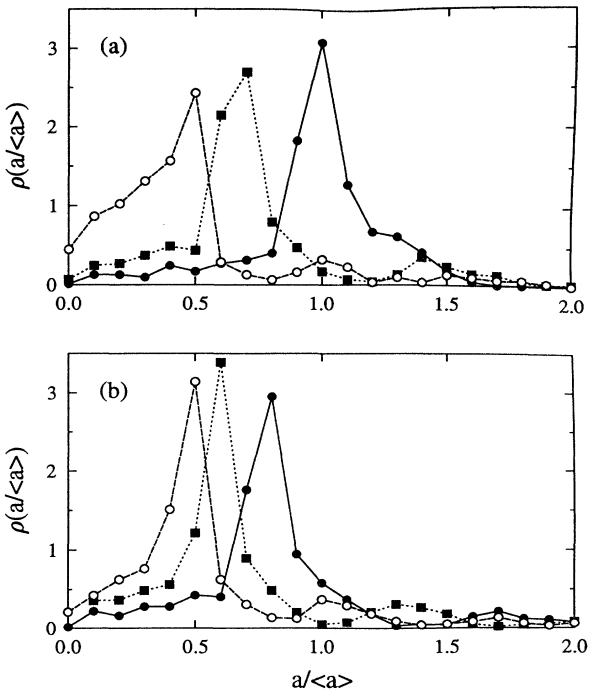


FIG. 11. (a) Distribution of normalized area, for medium ramping rate, in a dry breaking foam at various times during the breakdown cascade; ●, $t=490$ sec; ■, $t=690$ sec; ○, $t=890$ sec. (b) Same as (a) but over a narrow range of times; ●, $t=650$ sec; ■ $t=710$ sec; ○, $t=750$ sec.

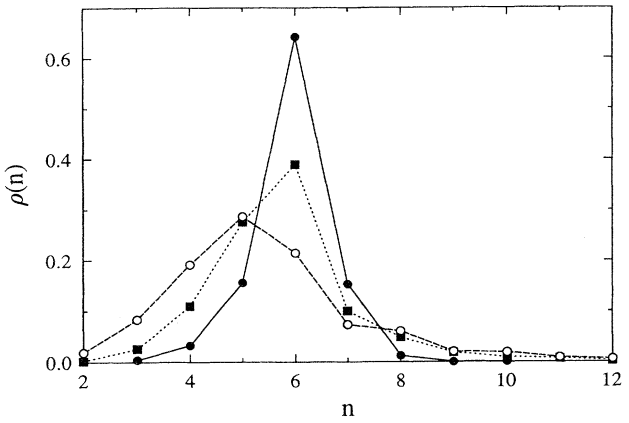


FIG. 12. Distribution of number of sides in a dry breaking foam, for medium ramping rate; ●, $t=390$ sec; ■, $t=690$ sec; ○, $t=790$ sec.

large numbers of sides which are surrounded by many small bubbles and, as such, give little insight into the mechanism of breakdown. If they are compared with those found for the other ramping rates there do not seem to be any obvious differences that could be used to distinguish the behavior of one rate from the other.

In addition to the cell area and side number we also analyze the behavior of the length $l$ of the sides making up a cell. Figure 13 shows $\langle l \rangle$ versus time, for all three ramping rates, revealing an essentially linear portion (fitted by the solid line) for a period of time after the break time. We believe that this linear behavior, so different from the expected square root dependence in the scaling regime of a nonbreaking foam, to be a very significant feature of the breakdown cascade. Figure 14 shows $P(l/\langle l \rangle, t)$ for the medium ramping rate, at a sequence of times over which $\langle l \rangle$ is linear. It should be noted that the histograms are not smoothed and although there is some variable spikiness in the center of the distributions the tails look quite steady, indicating that this distribution is effectively stationary in the linear growth period. If we go back to the

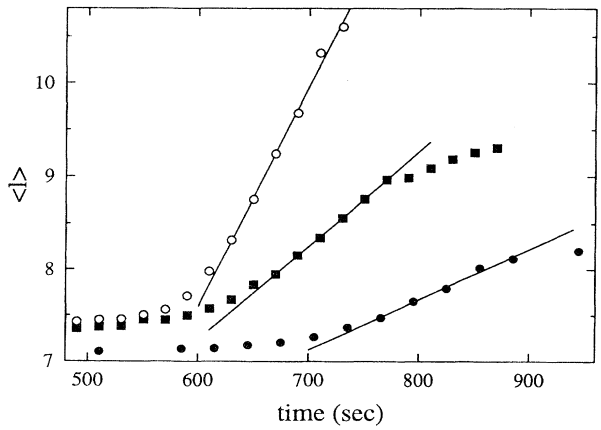


FIG. 13. Mean edge length as a function of time for the three ramping rates for a dry foam; ●, low ramping rate; ■, medium ramping rate; ○, high ramping rate. Solid line shows portion of curve well fitted by a straight line.

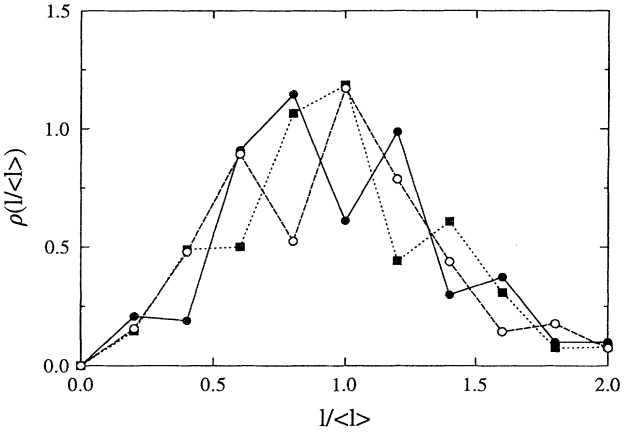


FIG. 14. Distribution of normalized side length, for medium ramping rate, in a dry foam during times corresponding to linear growth of $\langle l \rangle$; ●, $t=650$ sec; ■, $t=710$ sec; ○, $t=750$ sec.

area distributions $P(a,t)$ and look at these over the same time band [i.e., as shown in Fig. 11(b)] we see a distinct shift to the left. We comment that this contrasting behavior was also observed in our preliminary numerical modeling of the breakdown cascade [20].

The second moments of the various distributions such as the side number

$$\mu_2(n)=\sum_n (n-\langle n \rangle)^2 P(n,t) \tag{2}$$

and area

$$\mu_2(a)=\int (a-\langle a \rangle)^2 P(a,t)da \tag{3}$$

can be useful indicators of system "order." In Fig. 15 we show the evolution of $\mu_2(n)$ as a function of total bubble number for the middle ramping rate. The initial rapid in-

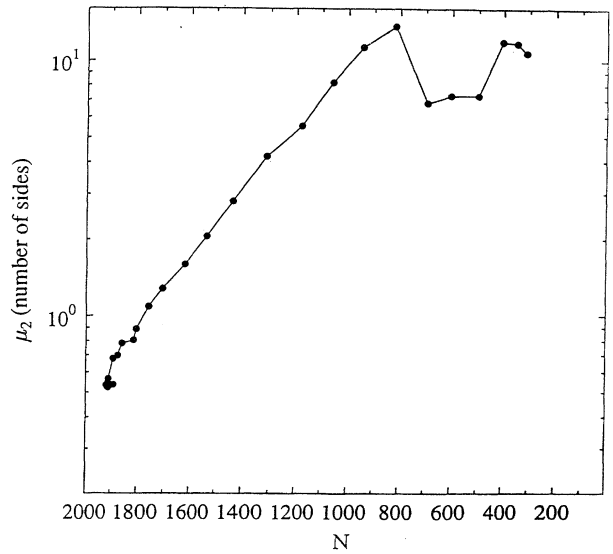


FIG. 15. Second moment of the number of sides as a function of the number of bubbles in a dry breaking foam for medium ramping rate.

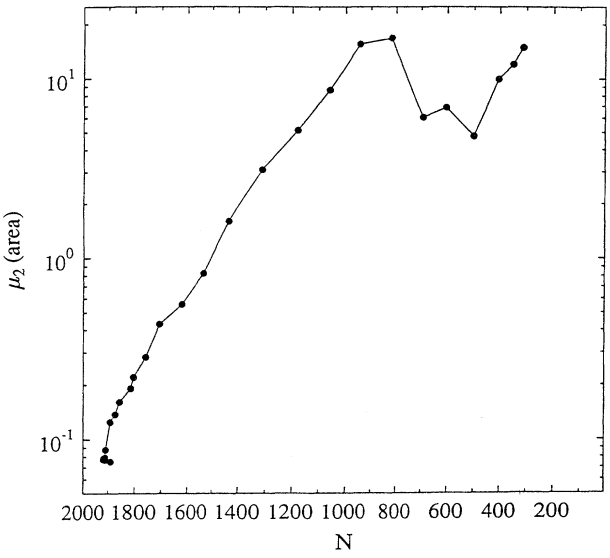


FIG. 16. Second moment of bubble area as a function of the number of bubbles in a dry breaking foam for medium ramping rate.

crease is consistent with the increasing disorder of the structure. The sudden drop and subsequent rise at smaller bubble number is a consequence of the breakup into disjoint regions and diminution of statistical quality associated with the drop in bubble number and appears to have little other significance. A similar type of behavior is also found for $\mu_2(a)$ as shown in Fig. 16. Although these second moment statistics do not seem to be particularly useful for breaking foams (as opposed to their value in characterizing nonbreaking foams) they provide additional benchmarks that are helpful for testing our numerical models [20].

## IV. DISCUSSION: A DIFFERENT SCALING REGIME

Developing a simple law to predict the break time as a function of ramping rate and initial conditions seems to be rather difficult. This is in no small part due to the complexities of the individual wall breakage mechanism. The structure, dynamics, and rupture of thin soap films has been the topic of study for a long time [21,22] although the body of work to date does not seem directly applicable to our case in which the bubble edges correspond to films that are both thin and narrow (corresponding to the plate separation in the cell). The recent lubrication theoretic approaches to study the breaking of individual, thick, films in Hele-Shaw [23] are also unlikely to be relevant. The weakening of our cell walls due to temperature ramping may well involve a number of complex and interrelated effects. Presumably there is an increase of fluid drainage along the walls towards the vertices (perhaps compounded by small scale convective motions), increased mobility of the soap molecules, and Marangoni effects. However, the dependence of the break time on initial bubble count and foam wetness may be manifestations of the same effect: namely, that bubble breakdown increases the wetness of the remaining bubbles and that initial distributions with fewer bubbles will take longer to achieve an equivalent degree of wetness than distributions with many smaller bubbles.

The breakdown cascade, by contrast, appears to be more amenable to analysis. For nonbreaking foams the relaxation is characterized by a scaling regime with stationary distributions of cell properties such as the normalized area distribution; namely, $P(a/\langle a\rangle,t)=P(a/\langle a\rangle)$. Since the process of relaxation is dominated by diffusion, as embodied by von Neumann's law, the only physical parameter controlling the evolution is the (effective) diffusion constant $\kappa$. Simple dimensional analysis tells us that length must scale as $(\kappa t)^{1/2}$ and hence area as $(\kappa t)^{1.0}$. As described in the Introduction, this linear growth law and stationarity of area distribution (and, indeed, all other distributions) is quite well established. The breaking dynamics occurs on a much faster time scale than the diffusive processes and $\kappa$ is no longer a relevant physical parameter. In the breakdown cascade the dominant process appears to be that of stress transmission through the network of cell walls. A realistic mechanical model for the motion of a bubble vertex, $r_i$, is of the form

$$\eta\frac{dr_i}{dt}=-\gamma\sum_j\frac{r_i-r_j}{|r_i-r_j|}\ , \tag{4}$$

where the sum is over the adjoining vertices [24]. The important point here is that the two physical parameters controlling the process are now $\eta$, the coefficient of friction per unit length of the soap film (here we assume the friction on the film, i.e., between the film and the top and bottom cell walls, to be isotropic and homogeneous), and $\gamma$, the surface tension. These parameters have dimensions $[\eta]=ML^{-1}T^{-1}$ and $[\gamma]=MT^{-2}$. Thus $[\gamma/\eta]=LT^{-1}$ sets the characteristic velocity scale from which we deduce that length must scale as $t^{1.0}$. We claim this is consistent with our observed behavior (see Fig. 13) of

$$\langle l\rangle\propto(t-t_b)^{1.0} \tag{5}$$

for $t>t_b$ where $t_b$ is the break time which depends on the ramping rate and other physical parameters of the system. Given such a scaling for $\langle l\rangle$ it is natural to investigate the behavior of the mean bubble area $\langle a\rangle$. In studying how $\langle a\rangle$ behaves as a function of time one is faced with the issue of how best to fit, on a log-log plot, the origin of time—on which results have been found to be quite sensitive [10]. Here we take an alternative approach which enables us to directly compare results for the different ramping rates. Rather than use time, we use bubble number $N$ as the measure of evolution. In Fig. 17 we plot, on a log-log scale for the three ramping rates, $\langle l\rangle$ versus $1/N$. Since $\langle a\rangle$ is defined as the total area (of the cell) divided by the bubble number $N$ at time $t$, we are thus able to compare $\langle l\rangle$ and $\langle a\rangle$ behavior directly. Making the best fit for the portions of the curves corresponding to the breakdown cascade we find that

$$\langle l\rangle\propto\langle a\rangle^{\alpha}\ , \tag{6}$$

where $\alpha=0.32$, 0.25, 0.28 for the high, medium, and low

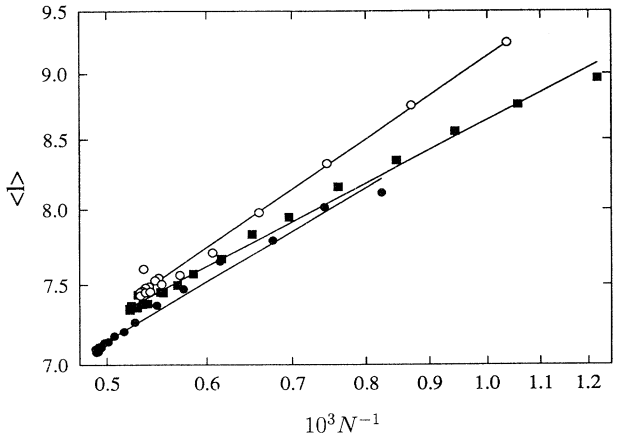


FIG. 17. Log-log plot of mean edge length versus inverse bubble number for the three ramping rates; ●, low ramping rate; ■, medium ramping rate; ○, high ramping rate.

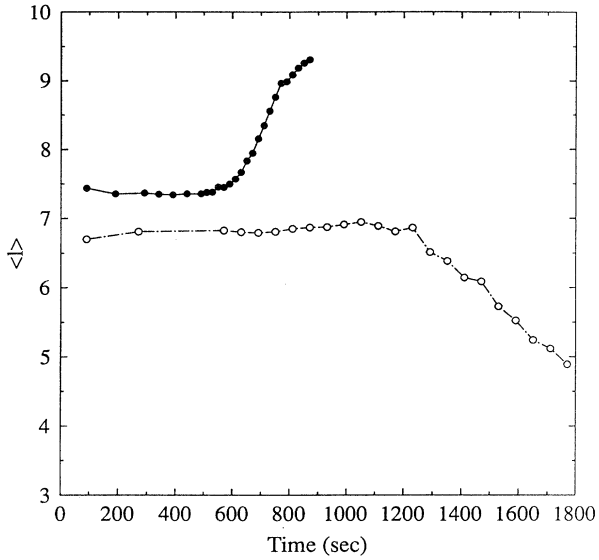


FIG. 18. mean edge length as a function of time for a wet (●) and dry (○) foam for same (medium) ramping rate.

ramping rates, respectively. Thus in the regions where $\langle l \rangle$ scales like $t^{1.0}$ we see that $\langle a \rangle$ scales like $t^{\beta}$ where $\beta = 1/\alpha = 3.12$, 4.00, 3.57 for the three different ramping rates. At first sight it might seem strange, since $\langle l \rangle$ scales like $t^{1.0}$, that $\langle a \rangle$ does not scale like $t^{2.0}$. However, this expectation is based on the experience of normal foam evolution in which it is natural to think of there being only *one* characteristic length scale (set by $\kappa$)—so that any quantity with the dimensions of length, such as the bubble edge length of the square root of the bubble area, should behave in the same way. In the case of a breaking foam, in which we see the creation of large area bubbles made up of many short edges, this no longer follows and, if anything, we would expect the area to scale as a higher power of edge length. This is what we see, but without universality, as manifested by the different exponents for the different ramping rates.

We conclude with an interesting observation concerning the effect of foam wetness on the dynamics of the breakdown cascade. In Fig. 18 we show, for the same ramping rate and approximately the same initial conditions, the evolution of $\langle l \rangle$ for the wet and dry foams. The striking feature is that after the break time (which, as expected, is much later for the wet foam) the wet foam shows a $\langle l \rangle$ behavior which is still approximately linear but now with a negative slope, i.e., the mean edge length is *decreasing*. This raises the intriguing possibility that in the breakdown cascade there might be a critical wetness for which $\langle l \rangle$ is approximately constant. This is clearly a topic for future investigations.

## ACKNOWLEDGMENTS

W.Y.T. acknowledges support from the Alfred P. Sloan Foundation and R.M.C.A. thanks the Program in Applied Mathematics at the University of Arizona for its hospitality. The authors thank D. Langevin for a valuable discussion concerning the properties and breakage of thin films and A. Bertozzi for other helpful comments.

[1] D. Weaire and N. Rivier, Contemp. Phys. **25**, 59 (1984).
[2] J. Stavans and J. Glazier, Phys. Rev. Lett. **62**, 1318 (1989).
[3] J. Glazier and J. Stavans, Phys. Rev. A **40**, 7398 (1989).
[4] J. Stavans, Phys. Rev. A **42**, 5049 (1990).
[5] H. Flyvbjerg, Phys. Rev. E **47**, 4037 (1993).
[6] H. Flyvbjerg, Physica A **194**, 298 (1993).
[7] J. Stavans, Physica A **194**, 307 (1993).
[8] J. Stavans, E. Domany, and D. Mukamel, Europhys. Lett. **15**, 479 (1991).
[9] M. Marder, Phys. Rev. A **36**, 438 (1987).
[10] T. Herdtle and H. Aref, J. Fluid Mech. **241**, 233 (1992).
[11] F. Bolton and D. Weaire, Phys. Rev. Lett. **65**, 3449 (1990).
[12] F. Bolton and D. Weaire, Philos. Mag. B **63**, 795 (1991).
[13] D. Weaire, F. Bolton, P. Molho, and J. Glazier, J. Phys. Condens. Matter **3**, 2101 (1991).
[14] J. Glazier, M. Anderson, and G. Grest, Philos. Mag. B **62**, 615 (1990).
[15] E. Holm, J. Glazier, D. Srolovitz, and G. Grest, Phys. Rev. A **43**, 2662 (1991).
[16] J. Glazier and D. Weaire, J. Phys. Condens. Matter **4**, 1867 (1992).
[17] J. Mombach, R. de Almedia, and J. Iglesias, Phys. Rev. E **47**, 3712 (1993).
[18] J. Mombach, R. de Almeida, and J. Iglesias, Phys. Rev. E **48**, 598 (1993).
[19] W. Tam and K. Szeto (unpublished).
[20] J. Chae and M. Tabor (unpublished).
[21] A. Sonin, A. Bonfillon, and D. Langevin, J. Colloid Interface Sci. **162**, 323 (1994).
[22] D. Wasan *et al.*, Prog. Surf. Sci. **39**, 119 (1992).
[23] A. Bertozzi and M. Pugh (unpublished).
[24] T. Nagai, K. Kawasaki, and K. Nakanura, J. Phys. Soc. Jpn. **57**, 2221 (1988).